INVERSE FREE ELECTRON LASER ACCELERATOR DEVELOPMENT

A. van Steenbergen*, National Synchrotron Light Source Department, and
Juan C. Gallardo, Physics Department, Brookhaven National Laboratory, Upton, NY 11973, USA

Abstract

The theoretical study of Inverse Free Electron Lasers (IFEL) as a potential mode of electron acceleration has been pursued at Brookhaven National Laboratory(BNL) for a number of years. As part of this program a proof-of-principle experiment with a single module accelerator unit has been recently successfully carried out. The IFEL accelerator made use of the 40 MeV linac beam and high power CO_2 laser beam of the Accelerator Test Facility (ATF), at BNL, in conjunction with a fast excitation , tapered period, wiggler. Basic aspects of the design of this single module IFEL accelerator will be presented, together with the experimental results of $\Delta E/E$ as a function of the IFEL parameters. Comparison with analytical and 1,3-D numerical simulations clearly establish the IFEL character of the electron - EM wave energy exchange, permitting thereby scaling to higher laser power magnitude and acceleration gradients. In addition, planned near term IFEL accelerator development will be indicated, incorporating the use of the IFEL as a beam prebuncher preceding a Inverse Cherenkov Accelerator, and the use of two IFEL modules in cascade in order to more realistically test the feasibility of a multi-module IFEL accelerator.

1 INTRODUCTION

The Free Electron Laser (FEL) uses a beam of relativistic electrons passing through a transverse, periodic , magnetic field (the *undulator*) to exchange energy with the coaxial propagating EM radiation field.[1] The FEL operates in such a manner that there is net energy transfer from the electron beam to the radiation field. Alternatively, net energy transfer from the radiation wave to the electrons is similarly possible. This concept, of using the FEL mechanism to effectively accelerate electrons, now called the Inverse-Free-Electron-Laser (IFEL) accelerator, is due to R. Palmer.[2] The basic principle of the IFEL accelerator is *identical* to that of the FEL, except that, in order to maintain resonance for optimum energy transfer, *tapering* of the undulator period length or its magnetic field is an added requirement. Early studies of IFEL[3, 4], clearly detailed the beam energy limitations of the IFEL accelerator, mainly related to synchrotron radiation energy loss at higher electron beam energies, and also uncovered possible favorable applications of the IFEL as a front end structure for alternative, non-conventional, accelerators. This has been the objective of recent BNL studies [5,6], aimed at the optimiza-

tion of the IFEL as a high gradient, single-module, accelerator cell as a first step toward a compact multi-module electron accelerator of maximum electron energy of a few GeV. IFEL proof-of-principle experiments have been carried out elsewhere, using a moderate power CO_2 laser source[7] and using a low power FEL with radiation wavelength of 1.65 mm as the driving beam [8]. More recently, experimental results of a single module IFEL, operating with a 1-2 GW CO_2 sapphire waveguide constrained laser beam and uniquely designed tapered period wiggler were reported.[9]

The theoretical description of IFEL interaction has been given by a number of authors. Here, we follow the basic formalism given in CPZ[4], with the further assumption that electron energy loss effect due to synchrotron radiation emission is taken to be zero and that the laser beam attenuation due to absorption by the accelerating electrons is negligible. The latter assumption is abandoned in further detailed treatment and, following KMR[10] a self consistent system of Lorentz equations for the electrons and the wave equations for the input laser field is used, to form the basis of both 1-D and 3-D IFEL computer simulations. With this the parameters for the, first experimental phase, IFEL single module test, were developed. This, together with the parameterization of beam wiggler and CO_2 guide, is given in section 2, below. First phase experimental results, together with IFEL simulation program results are presented in section 3, and a discussion of near term IFEL accelerator objectives is given in section 4.

2 IFEL EXPERIMENTAL ARRANGEMENT

Approximate analytical expressions, as derived in CPZ, together with the results of the 1-D simulation, were used to initially parameterize a single IFEL accelerator module. The parameters of the e- beam,[11] CO_2 laser beam[12] and IFEL wiggler are summarized in Tb.1; a schematic of the experimental configuration is given in Fig.1. For IFEL
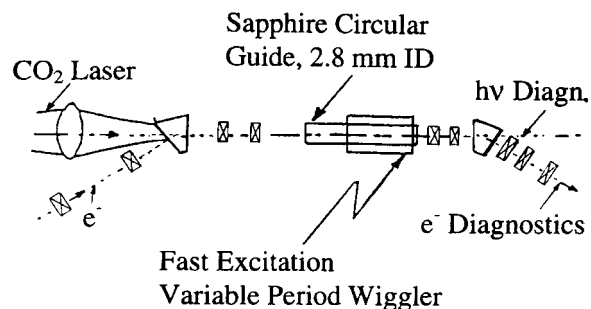

Figure 1: Schematic of the experiment configuration.

Table 1: IFEL first phase parameters.

e- beam		40.0	MeV
	Injection Energy	40.0	MeV
	Exit Energy	42.3	MeV
	<Accel.Field>	4.9	MV/m
	Current, nominal	5	mA
	N(bunch)	10^9	e-
	I(max.)	30	A
	$\Delta E/E(1\sigma)$	$\pm 3 \times 10^3$	
	Emittance (one σ)	7×10^8	m rad
	Beam radius	0.3	mm
Wiggler	Wiggler Length	0.47	m
	Section Length	0.6	m
	Period Length, λ_w	2.9–3.1	cm
	Wiggler Gap	4	mm
	Field max.	10	kG
	Beam oscill.,a1/2	0.16-0.2	mm
CO_2 Laser	Power, W_λ(Laser)	10^9	Watts
	Wavelength, λ	10.6	μ m
	Max.Field, E_o	0.78×10^3	MV/m
	Guide Loss, α	0.05	m^{-1}
	Field Attenuation	0.26	dB/sect.
	Pulse,(FWHM)	220	ps
	A_o	1.53×10^3	m^{-1}
	r_o ($L_w/2$)	1.0	mm

acceleration, it is necessary to maintain synchronism between the propagating electron beam and radiation wave, hence it is necessary to *taper* the wiggler. This can be accomplished by varying either the wiggler parameter K_w, the period length, λ_w or the maximum wiggler field, B_w . The choice is restricted by the maximum practical wiggler field and the minimum wiggler period length. It has been shown that, at low energy, maximum rate of acceleration, averaged over the full accelerator length, is obtained for a constant wiggler field accelerator.[5] Hence, for the IFEL accelerator of relevance here, the use of a period length tapered wiggler has been adopted. Although such a wiggler structure could be constructed using permanent magnets, the requirement of a specific period length taper would be costly and also difficult to subsequently change, in case higher laser power becomes available. Instead, for the present objective, a novel design fast excitation electromagnetic wiggler has been adopted[13, 14] which permits ready variation of the wiggler period length taper. This wiggler consists of stackable, geometrically alternating substacks of identical ferromagnetic (Vanadium Permandur [VaP]) laminations, in ($\frac{\lambda_w}{4}$) thickness substacks, separated by nonmagnetic laminations. Maximum achievable wiggler field, B_w, results from using conductive material for the nonmagnetic laminations, so that the induced fields from the eddy currents uncouple the wiggler *up* field from the *down* field. These *field reflectors* significantly enhance the maximum achievable field on axis.

A significant step towards design simplification of the single module IFEL accelerator, is the use of an extruded single crystal dielectric circular waveguide for the trans-

mission of the CO_2 radiation wave into the IFEL interaction domain. The design benefited from the pronounced progress that has been made in recent years in the development of waveguides for low loss transport of high power CO_2 laser beams. The type of guide adopted here for the objectives of the IFEL accelerator is the hollow-core dielectric guide, for which the core has a refraction index (vacuum, n=1) greater than the refraction index of the wall dielectric material ($n_{clad} < n_{core}$), resulting in solid fiber-like, low loss, behavior. As reported by Harrington and Gregory[16], a particularly favorable dielectric, with $n < 1$, for hollow guide CO_2 transport is Al_2O_3, either in the form of single crystal (SC) Sapphire or polycrystalline Alumina. As shown by Mercatelli and Schmeltzer(MS)[17], the attenuation constant, for the low order modes, is approximated by :

$$\alpha_{11} = (u_{11}/2\pi)^2 (\lambda^2/2a^3) Re[(\nu^2 + 1)/(\nu^2 - 1)^{1/2}] \quad (1)$$

where α, the attenuation coefficient, is defined by $P(z) = P(0)e^{-2\alpha z}$, $\nu = n - jk$ is the refractive index for the cladding material, [note, at $10.6\,\mu m$, $n = 0.67 - j0.03$], a is the circular guide radius, $2\pi/\lambda$ is the free space propagation constant and $u_{n,m}$ is the modal constant. For the fundamental mode, EH_{11}, $u_{1,1} = 2.406$. For the next low order mode EH_{12}, the modal constant equals 5.52, implying significantly greater attenuation for the CO_2 transport per unit guide length , hence reduced mode mixing, which is favorable for the present application. Various guide configurations were tested at low laser beam power with the beam focused to a Gaussian waist with adjustable radius at the entrance to the guide. For the 2.8 mm ID guide a laser power attenuation factor was measured of 0.2 dB/m. This is larger than predicted by the MS theory, but satisfactory for the IFEL accelerator application. Optimization of the coupling of the Gaussian mode laser beam into the desired EH_{11} propagating mode in the sapphire dielectric guide was done with the adoption of a entry matching cone and variation of the laser beam entry diameter. For optimum laser power transfer, a beam to guide aperture ratio of 0.74 is indicated theoretically[18] and was found to be valid experimentally. The CO_2 laser beam is directed through a ZnSe window into the coaxial $h\nu - e-$system, propagating as a free-space mode, to the circular dielectric waveguide. With deliberation, the dielectric guide was taken to be 0.6 m. in length, whereas the accelerator module length (wiggler length) was set at 0.47 m. This was done, together with the use of the guide entry cone, to approximate a mode matching section, enhancing thereby the mode purity in the IFEL module proper.

Beam transport from the exit of the linac to the e-diagnostic flag is designed to yield a dispersion free IFEL interaction region with a vertical betatron amplitude equal to the natural wiggler betatron amplitude of $\beta_x = 0.17\,m$. The IFEL e-acceleration is measured by means of a momentum spectrometer with adjustable local dispersion magnitude ($0.0 < \eta_p < 3.0\,m$), using a phosphor screen-vidicon camera-spiracon frame grabber.

3 IFEL EXPERIMENTAL RESULTS

In order to establish unambiguously correct overlap, both time wise and spatially, of the 300 ps CO_2 and 5 ps e^- beams, an observable interaction effect is an experimental necessity. To this end, therefore, the IFEL 1-D simulation code was used to yield the e- momentum distribution for the case of pronounced phase incoherence. The results suggested that, also in that case, the photon-e^- interaction would be measurable, so that synchronization could be established. With optimized matching of the e- beam and

Figure 2: Momentum spectrum of the unaccelerated and IFEL accelerated beam. E(e^-=34.2 MeV, B_w=0.82 T, $\lambda = 2.9 - 3.1$ cm, W_l =0.8 GW, $\Delta p/p = 2.2$ %.

CO_2 laser beam to the IFEL interaction region, optimization of the time synchronization of both beams, and correct interlacing of the lower repetition rate CO_2 laser pulse with the higher repetition rate e- beam pulses, e- IFEL acceleration was established. An example of the momentum spectrum of the unaccelerated and accelerated electrons is given in Fig.2, where the beam intensity distribution is shown versus $\sqrt{\beta_x \epsilon_x} + \eta_p \Delta p/p$, with the spectrometer optics adjusted so that $\eta_p \Delta p/p >> \sqrt{\beta_x \epsilon_x}$.

Optimization of the IFEL effect and exploration of parameter space, with variation of the electron beam injection energy, CO_2 laser power and wiggler maximum magnetic field magnitude was carried out in several consecutive runs, the results of which established the unambiguous signature
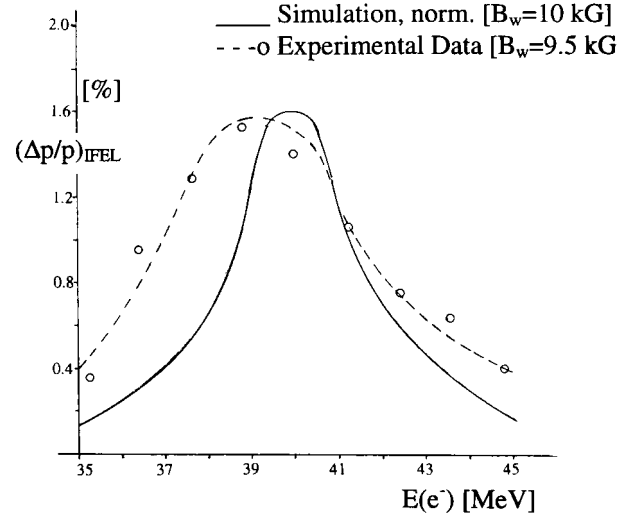
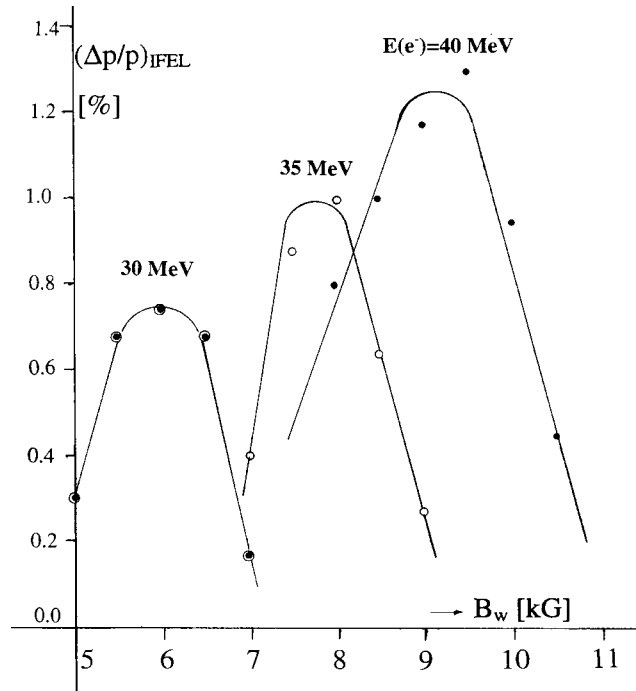Figure 3: Relative energy gain $\Delta p/p$. vs. E with B_w, W_l fixed.

Figure 4: Relative energy gain vs. B_w with E and W_l fixed.

4. In Fig.3 the relative energy gain $(\Delta p/p)_{\text{IFEL}}$ vs electron beam energy E for B_w and W_l constant, is shown, both as derived from the 1-D model simulations and as obtained experimentally, and in Fig.4 the relative energy gain vs B_w, for three beam energy values and W_l constant, is plotted. Although not shown in these figures, a maximum of $\Delta p/p = 2.5\%$ was measured with the parameters $E_e = 40$ MeV, $B_w = 10$ kG and $W_l = 1$ GW.

618

The approximate IFEL design equation[4] is:

$$\frac{d\gamma}{dz} = A\frac{K}{\gamma}f(K)\sin\psi \quad (2)$$

with $\psi = (k + k_w)z - kct$ and where the normalized laser electric field is $A = (e/mc^2)(1/R_o)\sqrt{\pi W_l Z_o}$, $K = (eB_w\lambda_w)/(2\pi mc) \approx 2.7$ is the wiggler parameter, $f(K) \approx 0.38$ is a correction factor due to the linear polarization of the wiggler, $Z_o = 377\Omega$, R_o is the waveguide radius and k, k_w are the radiation and wiggler wavevectors, respectively. The resonance condition leads to: $\lambda = 0.5\lambda_w/\gamma^2(1 + K^2/2)$. The relative energy gain of the electron beam in a wiggler of length L_w is:

$$\Delta\gamma/\gamma = (\Delta p/p)_{\text{IFEL}} = A(K/\gamma^2)f(K)\sin\psi_r L_w \quad (3)$$

where ψ_r is the resonance phase. The experimental results, as shown in Fig.3, agree well with the results obtained from the numerical simulations, with laser power $W_l = 1$ GW and the maximum wiggler field $B_w = 10$ kG, in $(\Delta p/p)$ magnitude normalized to the maximum experimental value. The experimental results given in Fig.4 also are in good agreement with precalculated values using the resonance condition, i.e. the observed B_w values for $(\Delta p/p)_{\text{MAX}}$ are $B_w = 9.2$ kG (40 MeV), 7.7 kG (35 MeV), 6.0 kG (30 MeV), yielding the λ_w values 3.06 cm, 3.05 cm and 3.11 cm, respectively, well within the design taper of the actual wiggler of $2.89 > \lambda_w > 3.14$ cm. With the present spectrometer, the energy gain could be measured with good accuracy due to the sharp intensity fall-off of the high energy edge of the non-accelerated particles. A quantitative intensity ratio of the accelerated to unaccelerated beam could not be obtained due to the extended low energy edge of the unaccelerated beam. This limited the ability to measure the bucket size and leakage for comparison with model predictions and therefore, the value of the synchronous phase angle ψ_r could not be unambiguously established. Analytically, ψ_r and $\Delta\gamma/\gamma$ as a function of laser power W_l and wiggler parameters are given by:

$$\sin\psi_r = \frac{3k}{16k_w}\frac{K}{Af(K)L_w}\left[(\frac{\lambda_w(L)}{\lambda_w(0)})^2 - 1\right]$$
$$\Delta\gamma/\gamma = 2\sqrt{\frac{Kf(K)A}{k(1+K^2/2)}}\Gamma(\psi_r) \quad (4)$$

These equations permit to calculate the moving bucket[10] parameter $\Gamma(\psi_r)$ and its maximum energy extent $\Delta\gamma/\gamma$. For the experimental value $\Delta\gamma/\gamma = 2.5\%$, it is found : $\psi_r = 34°$ in reasonable agreement with the optimal $45°$ and a laser power of $W_l = 2.7$ GW which is larger than the 1 GW estimated experimentally. In conclusion, the IFEL acceleration of a 40 MeV electron beam by $\Delta E/E = 2.5\%$ with a 1 GW CO_2 laser and a tapered wiggler with peak field on axis of 10 kG has been confirmed. Agreement with the model predictions is satisfactory, permitting the scaling of anticipated results to higher laser power.

4 IFEL ACCELERATOR OBJECTIVES

Present IFEL operation is limited to a maximum laser power of $< 2 - 3$ GW. With the objective of high energy

Table 2: IFEL two-module accelerator.

		M-I	M-II	
e beam	$E_{initial}$	40	76.7	MeV
	E_{exit}	76.7	106.3	MeV
Wiggler	Length	0.51	0.47	m
	λ_w	3.12-4.72	4.72-5.79	cm
	B_w	1	1	T
CO_2 laser	Power	100	100	GW
	pulse	10	10	ps
	Synchr. ϕ_r	50	50	°
	E_{MAX}	7.8	7.8	GV/m

gradient acceleration, high CO_2 laser power will be employed, initially at the 100 MW level, but with a longer term objective of 1 TW laser power. Hence, laser power damage to the dielectric guide wall is of concern. Assumed parameters are $W_l = 1$ TW, Effective Guide Cross Section $= 5.210^{-6}$m^2, or P/area$= 2.10^{13}W/cm^2$. Assuming lowest order mode transport only with the radial power density distribution approximated by a cosine function, and coaxial correct guide entry and transport, P/area at the guide wall is a factor of 10^6 smaller, hence the power density at the wall equals $\approx 210^7 W/cm^2$. For the present parameters, in a pulsed operating mode, this is a tolerable power density for the sapphire dielectric.

Near term further development of the IFEL accelerator concept will incorporate two approaches: **First**, the construction of a second VaP fast excitation wiggler - sapphire guide IFEL interaction region, for incorporation into a two accelerator modules IFEL accelerator, to test realistically a synchronized multi-module IFEL accelerator sequence and aim, with the above cited CO_2 laser developments, at a 100 MeV IFEL linac. The conceptual layout of this accelerator is shown in Fig.5 and the preliminary parameters are given in Tb2. Early results of IFEL particle transport simulation is given in Fig.6. Clearly, structure phase synchronization and minimization of bunch dilution in the inter cavity drift space demand appropriate, high resulution, bunch time measurement. The beam bunching factor produced by the IFEL interaction was measured using Coherent Transition Radiation (CTR).[19] **Second**, in a joint developmental approach with the STI Inverse Cherenkov Accelerator (ICA) experiment[20], use of the IFEL accelerator as a synchronized prebuncher for the IC accelerator in an IFEL-ICA buncher-accelerator sequence. Particle IFEL transport simulation has also been carried out for this application, as given in Fig.7, clearly evidencing the potential of the IFEL system to serve as a prebuncher for alternative modes of particle acceleration.
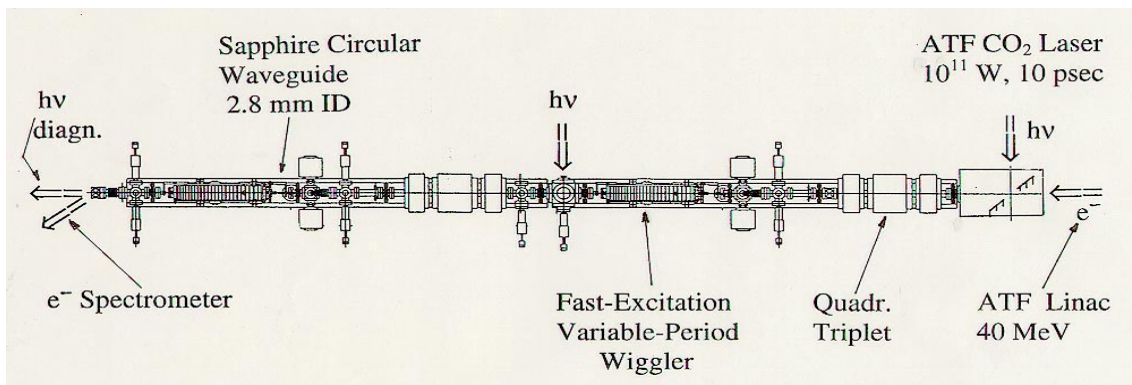
5 ACKNOWLEDGEMENTS

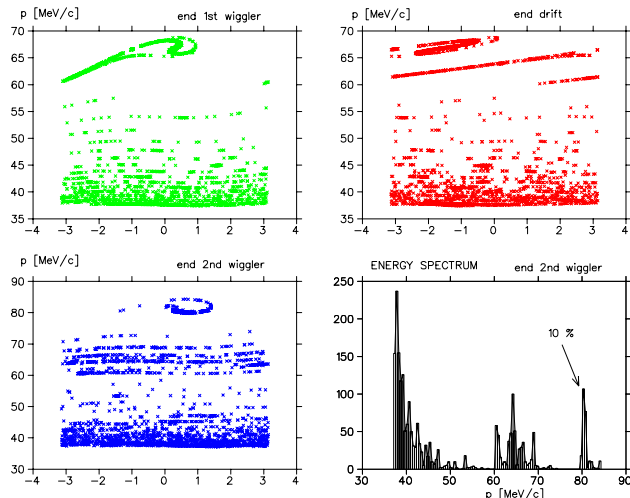Figure 5: IFEL two-module accelerator.

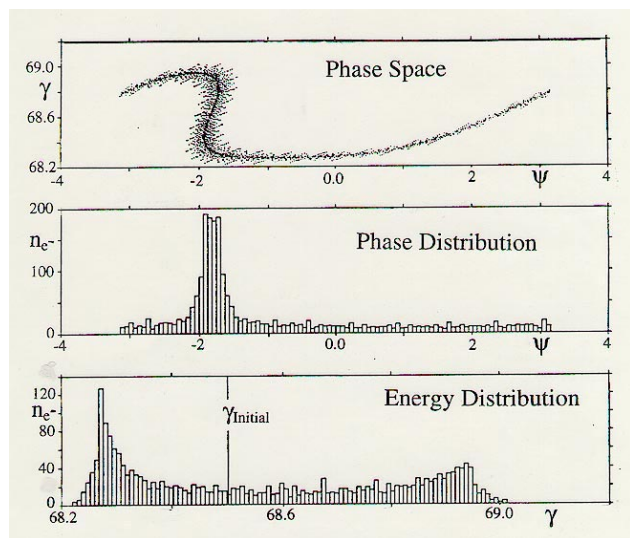Figure 6: IFEL two-module accelerator simulation.

Figure 7: Prebuncher simulation for the combined IFEL-ICA experiment. E=35 MeV, W_l=0.1 GW.

6   REFERENCES

[1] J. Madey, J. Appl. Phys. 42, 1906, 1971.

[2] R. Palmer, J. Appl. Phys. 43, 3014 ,1972.

[3] C. Pellegrini, P. Sprangle,W. Zakowicz, Proc. of the XIII Int.Conf. on High Energy Accelerators, p.473, 1983.

[4] E. Courant, C. Pellegrini, W. Zakowicz, Phys.Rev. A32, 2813, 1985.

[5] A. Fisher, J. Gallardo, J. Sandweiss, A. van Steenbergen, *Inverse Free Electron Laser Accelerator*, Proc. Adv. Accel. Concepts, Port Jefferson, NY, AIP 279, p.299, 1993.

[6] A. Fisher, J. Gallardo, A. van Steenbergen, J. Sandweiss, *IFEL Accelerator Development*, Nucl. Instr. Meth. A341, 1994.

[7] A. Amatuni et.al., Particle Accelerators 32, 221, 1990.

[8] I. Wernick and T. C. Marshall, Phys. Rev. A46, 3566 ,1992.

[9] A. van Steenbergen, J. Gallardo, J. Sandweiss, J. Fang, M. Babzien, X. Qiu, J. Skaritka, X-J. Wang , Phys. Rev. Let., Vol.77, 2690, 1996.

[10] N. Kroll, P. Morton, M. Rosenbluth, QE 7, 89, 1979.

[11] I. Ben-Zvi, Proc. Adv. Accel. Concepts, Port Jefferson, NY, AIP 279, 590, 1993.

[12] I. Pogorelsky, Proc. Adv. Accel. Concepts, Port Jefferson, NY, AIP 279, 608, 1993.

[13] A. van Steenbergen, Patent Application 368618, June 1989 (Issued Aug. 1990).

[14] A. van Steenbergen, J. Gallardo, T. Romano, M. Woodle, Proc. PAC, IEEE NS, May 1991.

[15] A. Fisher, J. Gallardo, A. van Steenbergen, J. Sandweiss, J. Fang, *IFEL Development*, AIP Conference Proceedings 335, editor P. Schoessow, AIP Press, 1995.

[16] J. Harrington, C. Gregory, Optics Letters 15, 1990.

[17] E. Marcatili, R. Schmeltzer, Bell System Techn. J., 43, 1783, 1964.

[18] K. Laakmann, W. Steier, Applied Optics, Vol.15, No.5, 1976.

[19] Y. Liu, X. J. Wang, M. Babzien, D. Cline, J-M. Fang, J. Gallardo, K. Kusche, I. Pogorelsky, J. Skaritka, A. van Steenbergen, *Experimental Results for IFEL Acceleration Micro-Bunching Measurement by CTR*, submitted to the Proc. of this Conference.

[20] W. Kimura, I. Pogorelsky, Y. Liu, K. Kusche, A. van Steenbergen, J. Gallardo, J. Sandweiss, D. Quimby, M. Babzien, *Inverse Cerenkov Acceleration using an IFEL Prebuncher*, submitted to the Proc. of this Conference.